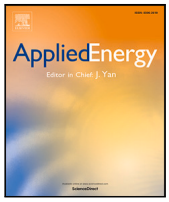
Applied Energy 376 (2024) 124337



Contents lists available at ScienceDirect

Applied Energy

journal homepage: www.elsevier.com/locate/apenergy



Dynamic model of integrated electricity and district heating for remote communities☆

Muhammad Abuelhamd [a,b,*], Claudio A. Cañizares [a]

[a] University of Waterloo, 200 University Ave. West, Waterloo, N2L 3G1, Ontario, Canada
[b] Assiut University, Assiut, 71515, Assiut, Egypt

ARTICLE INFO

Keywords:
District heating network
Frequency control
Heat pump
Integrated electricity and heating network
Microgrid
Remote communities

ABSTRACT

District heating networks offer promising solutions for remote communities, providing centralized heat supply, improved efficiency, and diverse energy sources, especially with existing diesel generation. Hence, this paper bridges gaps in the existing literature by developing comprehensive dynamic models of combined district heating networks within existing electric power networks in remote communities, which allows identifying challenges and benefits of district heating networks for these communities. It is shown that district heating networks allow utilizing waste energy to enable energy exchanges between the electricity and heating systems, enabling the provision of necessary ancillary services for remote microgrids with renewable energy sources. The presented dynamic district heating network model incorporates particular considerations in remote, northern communities such as soil limitations, extreme cold conditions, and piping insulation to minimize heat loss. It also addresses accurate sizing of heat pumps based on realistic thermal load requirements, weather conditions, and consumer profiles, proposing demand management controls to enhance frequency regulation for the integration of variable renewable energy sources. The main contributions of the paper include detailed dynamic modeling for district heating network operation, heat pump demand response control system design, and a comparative analysis between centralized district heating networks and decentralized electric thermal storage units that have been deployed for thermal supply in remote areas. The presented dynamic models are applied, tested, and validated in an existing electric microgrid at Kasabonika Lake First Nation in Northern Ontario, showcasing the role of a potential district heating network in facilitating renewable energy sources integration in isolated microgrids.

1. Introduction

The energy transition to net-zero is a global priority, with Canada aiming to achieve zero CO_2 emissions by 2050 [1]. In this context, District Heating Networks (DHNs) are a promising solution, offering centralized heat supply for multiple buildings, enhancing efficiency, utilizing diverse energy sources, and minimizing infrastructure needs [2]. While DHNs involve higher initial costs, their scalability and long-term savings make them attractive to improve energy efficiency. This is particularly true for remote, northern communities, which have significant thermal loads associated with their northern location and present a pressing need for the integration of Renewable Energy Sources (RES) into their Electrical Power Network (EPN) to significantly reduce emissions, as discussed in [3]. This is an urgent concern for these communities, where the rate of warming is 3 to 4 times that of the rest of the planet, with local emission and soot from Diesel Generators (DGs) having a direct impact on ice melting. Thus, in these communities, DHNs are regarded as an attractive solution to supply their thermal needs (e.g., [4–6]). For example, the authors in [4] study implementing biomass-driven DHNs in northern remote and rural communities, demonstrating that biomass-driven DHNs offer economic benefits for remote and rural energy systems. In [5], the estimated cost of delivering heat through biomass-driven DHNs is shown to be lower than the estimated price of fuel oil in rural villages. In [6], the authors analyze a Combined Heat and Power (CHP) microgrid for remote communities, with integrating renewable energy to reduce diesel consumption and energy costs. These research papers explore the economic feasibility of implementing DHNs in remote communities; however, there is a notable gap in addressing the dynamic feasibility and challenges of DHNs in such areas, which is the focus of the current paper.

☆ The language editing tool ChatGPT was employed for editing purposes.

* Corresponding author.
E-mail addresses: ma7mahmo@uwaterloo.ca (M. Abuelhamd), ccanizar@uwaterloo.c (C.A. Cañizares).

https://doi.org/10.1016/j.apenergy.2024.124337
Received 7 May 2024; Received in revised form 6 August 2024; Accepted 25 August 2024
Available online 3 September 2024
0306-2619/© 2024 The Author(s). Published by Elsevier Ltd. This is an open access article under the CC BY-NC license (http://creativecommons.org/licenses/by-nc/4.0/).

Nomenclature

Acronyms

CFHX	Counter Flow Heat Exchanger
CHP	Combined Heat and Power
COP	Coefficient Of Performance
DG	Diesel Generator
DHN	District Heating Network
EG	Exhaust Gas
EPN	Electrical Power Network
ETS	Electric Thermal Storage
GHG	Green-House Gas
GIS	Geographic Information Systems
HP	Heat Pump
HVAC	Heating, Ventilation, and Air Conditioning
HX	Heat Exchanger
IEHS	Integrated Electricity and Heating System
IM	Induction Motor
KLFN	Kasabonika Lake First Nation
QOS	Quality Of Service
RES	Renewable Energy Source
SRLS	Smart Residential Load Simulator
TRV	Thermostatic Radiator Valve
VSC	Voltage Source Converter
WG	Wind Generator

Parameters

A	Normalized house area [m^2]
A_{HX}	HX surface area [m^2]
A_p	Pipeline control volume surface area [m^2]
C_{ins1}	First layer insulator heat capacity [J/°C]
C_{ins2}	Second layer insulator heat capacity [J/°C]
C_{rdh}	Radiator thermal capacity [J/°C]
C_{st}	Carbon steel heat capacity [J/°C]
C_w	Water heat capacity inside pipeline [J/°C]
h	Convective heat transfer coefficient between feed water and pipe wall [W/m^2 °C]
k	TRV regulation constant
$k_{DR1,2,3}$	ETS demand response adjustment constants
k_{ins1}	First insulator thermal conductivity [W/m °C]
k_{ins2}	Second insulator thermal conductivity [W/m °C]
k_s	Soil thermal conductivity [W/m °C]
k_{st}	Carbon steel thermal conductivity [W/m °C]
k_w	Water thermal conductivity [W/m °C]
L_p	Pipeline control volume length [m]
r_1	Pipeline inner radius [m]
r_2	Carbon steel layer radius [m]
r_3	First insulator layer radius [m]
r_4	Second insulator layer radius [m]
R_{rdh}	Radiator hot side resistance [°C/W]
R_{rdr}	Radiator cold side resistance [°C/W]
S_H	House number of floors
Z	Pipeline depth [m]
$\overline{P}_{DR}$	ETS peak power at a given time [W]
τ_{HP}	Reference HP induction motor torque [N m]

Variables

COP	HP coefficient of performance [p.u.]
C_r	Fluids heat capacity rate ratio in HX [p.u.]
Δf	Frequency deviation [Hz]
$\dot{m}_w$	Water mass flow rate [Kg/s]
f	Frequency [Hz]
f_o	Reference frequency [Hz]
f_v	TRV control function [Kg/s]
K_i	Integral controller gain
K_p	Proportional controller gain
NTU	Number of transfer units for HX [p.u.]
P_{EHth}	Thermal power of an electric heater unit [W]
P_{EHe}	Electric power of an electric heater unit, [W]
P_{HPe}	HP electrical power [W]
P_{HPth}	HP thermal power [W]
P_{Hth}	House thermal power [W]
Q	Transferred power between HX fluids [W]
Q_{rd}	Radiator thermal power [W]
$Q_{w,st}$	Pipeline heat loss transferred from water to carbon steel layer [W]
τ_{HP}	Reference HP induction motor torque, [N m]
T_a	Ambient temperature [°C]
T_{mix}	Mixer resultant temperature [°C]
T_{HPin}	HP inlet temperature [°C]
T_{HPout}	HP outlet temperature [°C]
T_{HXcin}	Cold fluid inlet temperature of the HX [°C]
T_{HXhin}	Hot fluid inlet temperature of the HX [°C]
T_{ins1}	Temperature of first layer insulator [°C]
T_{ins2}	Temperature of second layer insulator [°C]
T_{ph}	Pipeline hot temperature [°C]
T_{rdh}	Radiator hot side temperature [°C]
T_{rdr}	Radiator return water temperature [°C]
T_{st}	Temperature of carbon steel layer [°C]
T_{wh}	Hot water temperature inside pipelines [°C]
T_S	Space temperature [°C]
ε	Effectiveness of HX
ω_{HPo}	Reference speed of HP induction motor [W]
ψ	HP second-law efficiency [p.u.]
$\mathbb{1}$	Vector of ones

Implementing DHNs in remote communities presents unique challenges due to geographical isolation, harsh environmental conditions, and limited infrastructure. Despite these difficulties, the idea is gaining traction, with several pilot projects demonstrating its feasibility. For instance, the U.S. Department of Energy supports isolated communities with geothermal DHN projects, like the one in Nome, Alaska, aimed at reducing carbon pollution and lowering utility bills. These projects show that, although in its early stages, DHNs can provide sustainable and efficient heating solutions for remote areas [7].

The dynamic operation of the DHN in remote communities encompasses special considerations such as piping network design, insulation requirements, burial depth specifications, and the unique challenges

posed by low linear heat density and extremely cold ambient temperatures. Thus, an accurate assessment of DHN feasibility in remote regions necessitates a thorough understanding of the DHN detailed dynamic modeling. In this context, this paper aims to investigate the dynamic modeling of utilizing waste energy from a diesel engine's exhaust to power a DHN in remote communities, considering that existing static and optimization models, like for example [6], lack the ability to properly represent the piping network characteristics and thermal loads' capacity within the DHN. Furthermore, the dynamic modeling allows to study the integration of Heat Pumps (HPs), considering their ratings and the required number of units to meet thermal demands, along with comprehensive design considerations for all DHN components in remote communities. Therefore, the dynamic studies presented here are a novel contribution to the existing literature, as detailed dynamic operation of DHNs in remote communities has not been addressed previously. It is important to note that this paper does not address the economic aspects of DHNs in remote communities, which have been discussed in the existing literature.

On the other hand, there has been a growing trend towards electrical and thermal systems integration to achieve optimal operation of the combined systems and minimize GreenHouse Gas (GHG) emissions [8]. Therefore, the presented work also aims to study the integration of DHNs with the EPN in remote communities, facilitating efficient energy exchange between the two networks by managing HP demand to provide frequency control for the EPN while ensuring the required Quality Of Service (QOS) for DHN customers, which has not been studied in the existing literature for remote microgrids. Assessing the QOS in a DHN, particularly under secondary frequency control, requires developing a detailed dynamic model of the DHN to accurately incorporate the characteristic of the DHN, particularly in remote communities where DGs are redispatched every 15 min [9]. This interval is significant for the DHN, particularly in the presence of HPs.

The dynamic modeling works of Integrated Electricity and Heating Systems (IEHSs) with DHNs for EPN studies are limited, especially for remote microgrids, as previously mentioned. Furthermore, the benefits of DHNs for remote communities, where waste heat from DGs can be exploited, has not been reported in the context of microgrids while considering the DHN dynamics. Thus, several studies have explored diverse strategies aimed at reducing GHG emissions while simultaneously providing ancillary services when integrating DHNs in EPNs based on static DHN models. For example, in [10], a control strategy for a DHN is developed to minimize electric energy consumption from pumping in the Dark Landing Solar Community in Alberta, aiming to reduce GHG emissions associated with fossil fuel-based electricity generation in remote microgrids. The authors in [11] introduce a co-generation system using a small modular reactor for district heating and frequency regulation in the presence of variable RESs. Different case studies are discussed in [12], where the potential of DHNs to provide balancing services in the European Union is explored. Ref. [13] demonstrates that distributed circulating pumps with variable speed motors are more efficient than central circulating pumps, indicating the possibility of saving electric energy for ancillary reserve power in EPNs. All these references are based on static DHN models suitable for dispatch studies, without accounting for relevant DHN dynamic behavior.

A dynamic model of an IEHS is crucial for proper system integration, particularly control and energy management. To accurately represent the dynamic response of combined heating and electricity systems, it is necessary to model each major component individually and interconnected, especially for remote communities where the extreme cold temperatures present challenges for the control and operation of DHNs; in fact, existing models oversimplify crucial dynamics. For instance, in [14], an equivalent circuit model for the DHN is proposed without considering relevant dynamics like pipe losses and thermal energy storage in pipe insulators. In [15], the authors introduce an integrated heat and power dispatch model without fully accounting for piping insulation systems or the thermal inertia of consumers. Ref. [16] develops a non-iterative equivalent model for the IEHS, focusing solely on the DHN primary circuit and simplifying the representation of the secondary circuit. In [17], the DHN model also neglects the representation of piping insulation. Moreover, Refs. [14]–[17] provide the thermal demand as a total aggregated demand, which overlooks the need for disaggregation to understand DHN operations and the impact of thermal fluctuations on the QOS for consumers. Finally, all these references consider a time resolution of hours, which is not sufficient to test the interaction of the DHN and EPN systems to properly understand the relevant dynamics of the IEHS studied in the current paper.

There are various references in the literature discussing the DHN and its benefits for frequency regulation. For example in [18], the authors study a combined small modular reactor and DHN to manage electric load fluctuations in EPNs, enhancing RES integration and grid stability. However, the study does not consider the DHN's secondary circuit dynamics, using 15 min resolution that does not allow to consider primary frequency regulation issues. Ref. [19] analyzes the dynamic operability of interconnected CHP plants and DHN for flexible power generation, but the models utilized are not detailed enough to properly capture frequency regulation phenomena. The authors in [20] propose a model-based approach to assess the potential of power-to-heat assets for frequency regulation. However, the simplified representation of the DHN in the case study does not fully capture the necessary IEHS dynamics. In [21], a state space model is proposed to represent large-scale HPs in DHNs, enabling performance evaluation of local frequency control methods, highlighting the HPs promising role in IEHS, but there is no proper modeling of the EPN to study the required IEHS dynamics relevant to frequency control.

To address the modeling gaps previously identified for the proper dynamic studies of the DHN and IEHS, especially in the context of remote communities, the present paper develops a detailed physical model for realistic integrated DHN and EPN systems in the context of remote microgrids, which enables a proper examination of the feasibility and challenges of the combined systems' dynamic performance in isolated microgrids. Thus, the main contributions of this paper can be summarized as follows:

- The developing of dynamic models to analyze the feasibility and challenges of the use of waste energy from a diesel engine's exhaust to power a DHN for the provision of thermal heating in remote microgrids, considering soil limitations, extreme cold temperatures, and the minimization of heat loss through proper piping insulation, as well as the proper sizing of HPs to meet thermal load requirements that account for weather conditions, the EPN characteristics, and the consumers' thermal needs.
- The design of a control system for HP demand response to study the provision of reserve power for the EPN to enhance frequency control in remote microgrids.
- The demonstration of the advantages of using DHNs for integration of variable RESs into the EPN of isolated microgrids to mitigate their adverse dynamic effects, based on a simulated model of a DHN and an actual model of an EPN at an existing remote microgrid, including a comparison between centralized DHNs and decentralized Electric Thermal Storage (ETS) units to supply the community's thermal demand, and their potential application for EPN frequency control through HP demand regulation or ETS demand response strategies.

The rest of the paper is organized as follows: Section 2 focuses on the detailed dynamic modeling and control of a DHN in remote communities, demonstrating the feasibility and challenges of using DG heat waste to provide the community thermal needs. The design of a DHN for the Northern Ontario community of Kasabonika Lake First Nation (KLFN) is also discussed in this section. Section 3 discusses the utilization of the DHN for providing frequency support in a microgrid through HP and ETS demand control, comparing their application and benefits for a realistic IEHS in the KLFN community. Section 4 highlights the main contributions and conclusions of the presented studies.

2. DHN model

An IEHS requires the integration of multiple components to meet the electricity and heating demands of a community. This section discusses the essential elements of a DHN in a remote community IEHS, considering for the first time relevant thermal system dynamics, and demonstrates and discusses its application to the KLFN community.

2.1. Household model

The Smart Residential Load Simulator (SRLS) tool has been used here for studying IEHS in smart grids [22]. The package contains detailed models of appliances, Heating, Ventilation, and Air Conditioning (HVAC) systems, and thermal components in homes. In this paper, this tool is utilized to model the individual household thermal dynamics, which is a fundamental component of a DHN. In this context, replacing the heating source from individual furnaces with a DHN heat supply in a household requires detailed modeling of a radiator and its control, as detailed in [23]. Additionally, the representation of temperatures resulting from mixing multiple mass flow rates at different temperatures within a household is needed [24].

Based on [25], a typical Canadian household consists of four main spaces with varying dimensions and thermodynamic properties. In the context of a DHN, each space is presumed to have different radiator capacity corresponding to its heating area, with hot water being distributed among the radiators, starting from the inlet pipeline at the house's entrance and mixed at the outlet pipeline. Consequently, the household model for DHN studies comprises individual models for each space, along with a mixer model that calculates the resultant temperature after combining the mass flow rates and corresponding temperatures of the four spaces. The thermal dynamics of such a household can be modeled using proper models and simulation tools, as described in detail next.

2.1.1. Single space model

The dynamic thermal model of a single space in the SRLS is described in some detail in [22], based on an electric circuit model that represents the thermal dynamics of the area. In this model, the radiator can be readily integrated by adding the following equations [23]:

$$\frac{dT_{rdh}}{dt} = \frac{T_S - T_{rdh}}{C_{rdh}R_{rdh}} + \frac{Q_{rd}}{C_{rdh}} \tag{1}$$

$$Q_{rd} = c_w \dot{m}_w (T_{ph} - T_{rdh}) \tag{2}$$

$$\frac{dT_{rdr}}{dt} = \frac{T_{rdh} - T_{rdr}}{C_{rdh}R_{rdr}} \tag{3}$$

where all variables and parameters in these and other equations are defined in the Nomenclature section. It is assumed that T_{rdh} and T_{rdr} are approximately the same, which allows the radiator's virtual resistance $R_{vr} = \frac{1}{c_w \dot{m}w}$ in (2) to be included in the space's electric circuit model.

To simulate Thermostatic Radiator Valve (TRV) operation and control hot water flow rate, the following function can be utilized:

$$f_v = \frac{\dot{m}_{max}}{1 + e^{-k(T_{So} - T_S)}} \tag{4}$$

In this study, only conductive thermal resistances are considered, assuming a uniform space temperature.

2.1.2. House and mixer models

The household thermal dynamic model consists of individual models for each of the four spaces, assuming that the return mixed temperature can be described as follows [24]:

$$T_{mix} = \frac{\sum \dot{m}_w T_{rdr}}{\sum \dot{m}_w} \tag{5}$$

The household model takes into account the internally generated thermal power, as well the solar irradiation considering all surrounding directions (south, north, east, west, and roof), based on the equations described in [22], which discusses in some detail the thermal heat generated from solar irradiation on the household used in the present work. It assumes that heat from solar radiation passing through windows and impacting external walls is stored in the room's internal thermal mass and external walls' thermal mass, respectively. This model requires specific input data: beam irradiance (W/m^2), diffuse irradiance (W/m^2) for a specific day of interest throughout the year, and the latitude of the location under study. The model has been implemented in the SRLS tool used in the paper [25], which is a Matlab-Simulink-GUIDE tool that facilitates the study of energy management systems in smart grids.

2.2. Pipeline heat loss

The household dynamic thermal model is a fundamental component of the DHN's secondary circuit. This model is integrated into the DHN, which also includes pipelines to form a heat distribution network with both hot- and cold-water flows to deliver thermal power from the heat sources to individual consumers. Accurate modeling of the pipelines, including considerations for insulation and pipe material, is crucial to capture the dynamics of stored energy within the pipes. Proper modeling of pipelines is essential to represent thermal losses and temperature variations accurately, with the diameters of these pipelines playing a significant role. These pipelines can be efficiently designed using Geographic Information Systems (GIS) and thermal network design tools, which allow estimating mass flow rates, heat loss, and temperature drops within the heat distribution network, ensuring efficient thermal power delivery to households.

The following equations govern the pipeline model [26]:

$$C_w\left(\frac{dT_{wh}}{dt}\right) = (T_{ph} - T_{wh})c_w \dot{m}_w + Q_{w,st} \tag{6}$$

$$C_{st}\left(\frac{dT_{st}}{dt}\right) = \frac{T_{ins1} - T_{st}}{\frac{ln(r_2/r_1)}{2\pi k_{st} L_p}} - Q_{w,st} \tag{7}$$

$$C_{ins1}\left(\frac{dT_{ins1}}{dt}\right) = \frac{T_{ins2} - T_{ins1}}{\frac{ln(r_3/r_2)}{2\pi k_{ins1} L_p}} - \frac{T_{ins1} - T_{st}}{\frac{ln(r_2/r_1)}{2\pi k_{st} L_p}} \tag{8}$$

$$C_{ins2}\left(\frac{dT_{ins2}}{dt}\right) = \frac{T_a - T_{ins2}}{\frac{ln(r_4/r_3)}{2\pi k_{ins2} L_p} + \frac{ln(2Z/r_4)}{2\pi k_s L_p}} - \frac{T_{ins2} - T_{ins1}}{\frac{ln(r_3/r_2)}{2\pi k_{ins1} L_p}} \tag{9}$$

$$Q_{w,st} = \begin{cases} hA_p(T_{st} - T_{wh}) & \text{if } \dot{m}_w > 0 \\ 8\pi k_w (T_{st} - T_{wh}) & \text{if } \dot{m}_w = 0 \end{cases} \tag{10}$$

$$R_1 = \frac{ln(r_2/r_1)}{2\pi k_{st} L_p} \tag{11}$$

$$R_2 = \frac{ln(r_3/r_2)}{2\pi k_{ins1} L_p} \tag{12}$$

$$R_3 = \frac{ln(r_4/r_3)}{2\pi k_{ins2} L_p} + \frac{ln(2Z/r_4)}{2\pi k_s L_p} \tag{13}$$

These equations describe the behavior and dynamics of the pipeline system using the electric-circuit analogy, with Fig. 1 illustrating an electric circuit model of a specific pipeline control volume.

The underlying principles and equations governing heat transfer and temperature dynamics apply to both the hot and cold sides of the system. Therefore, the aforementioned equations can be utilized to model and analyze the behavior of the entire pipeline network, regardless of whether it pertains to hot or cold water.

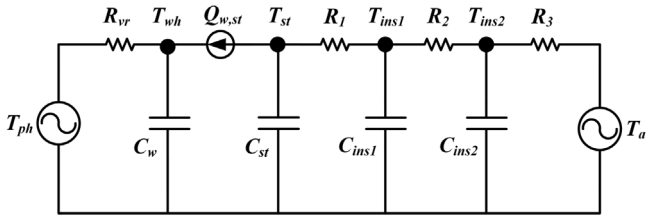


Fig. 1. Electric equivalent circuit of the pipeline control volume.

2.3. Heat exchanger

The Heat Exchanger (HX) is a vital component in DHNs that transfers heat between fluids of different temperatures. It facilitates efficient heat transfer from the primary circuit, where heat is generated, to the secondary distribution circuit for heating purposes. Different types of HXs are used in DHNs [27]. Here, the design aspects of the Counter Flow HX (CFHX) are discussed for a given generated thermal power capacity, considering the Exhaust Gas (EG) peak thermal power. Thus, the CFHX can be effectively modeled using the effective number of transfer units (effective-NTU) method, which involves the following equations [28]:

$$Q = \varepsilon \underline{C}(T_{HXhin} - T_{HXcin}) \tag{14}$$

$$\varepsilon = \begin{cases} \frac{1-e^{(-NTU(1-C_r))}}{1-C_r e^{(-NTU(1-C_r))}} & \text{if } C_r = \underline{C} \,/\, \overline{C} < 1 \\ \frac{NTU}{1+NTU} & \text{if } C_r = 1 \end{cases} \tag{15}$$

$$NTU = \frac{U_{HX} A_{HX}}{\underline{C}} \tag{16}$$

2.4. Thermal power plant

A thermal heat source serves as the primary energy source for the DHN. Common examples include CHP plants, biomass boilers, and geothermal energy. In this paper, the focus is on utilizing waste heat from the EG of diesel engines in remote communities as the primary heat source. However, during peak thermal demand, the power generated from the EG recovery system may be insufficient to meet the consumers' temperature requirements. Hence, HPs are employed to compensate for the thermal power shortage. The integration of the EG recovery system and a single HP, which is likely sufficient in a remote community, given their relatively small footprint, forms the thermal power plant for the DHN. The main thermal power model comprises three components: an EG mass flow rate $\dot{m}_{gas}$ and temperature T_{gas} model, a HX model, and a mass flow rate control model. Each of these components, which are discussed next, can be characterized by detailed quasi-dynamic models, including the HP model as an integral part of the DHN thermal plant.

2.4.1. Diesel exhaust gas

The thermodynamic properties of the EG can be accurately modeled by utilizing the tabular data provided by the manufacturer for DGs of different power ratings. Thus, using curve fitting techniques, the EG mass flow rate and temperature can be expressed as functions of the generator electric loading condition P_{gen} as follows:

$$\dot{m}_{gas} = -2{P_{gen}}^2 + 3.836 P_{gen} + 3.925 \tag{17}$$

$$T_{gas} = -21.6{P_{gen}}^2 + 139.9 P_{gen} + 412.1 \tag{18}$$

The density of the EG is typically assumed to be 1.33 kg/m^3 based on experimental studies in [29], while the specific heat capacity of the EG is assumed to be 1.005 KJ/Kg °C [30]. In order to regulate the mass flow rate of the EG, a proportional controller can be employed.

2.4.2. Heat pump

To compensate for any shortage in the generated thermal power, an electricity-driven HP is necessary. The average model of the HP can be described using the following equations, based on [31–33] , starting with the HP COP based on the Carnot cycle:

$$COP_{max} = \frac{T_{hot}}{T_{hot} - T_{cold}} \tag{19}$$

$$COP = \psi \cdot \frac{T_{hot}}{T_{hot} - T_{cold}} \tag{20}$$

$$T_{hot} = \frac{T_{HPin} + T_{HPout}}{2} \tag{21}$$

$$T_{cold} = T_a \tag{22}$$

$$COP = \psi \cdot \frac{\frac{T_{HPin}+T_{HPout}}{2}}{\frac{T_{HPin}+T_{HPout}}{2} - T_a} \tag{23}$$

However, as per the Carnot theorem, all temperatures in the COP equation should be absolute temperatures in K, which can be converted to °C as follows:

$$COP = \psi \cdot \frac{(T_{HPin} + T_{HPout})/2 + 273.15}{(T_{HPin} + T_{HPout})/2 - T_a} \tag{24}$$

where COP is a dimensionless quantity. Additionally, the heat gained by the water through the HP P_{HPth} increases its temperature by ΔT as follows:

$$COP = \frac{P_{HPth}}{P_{HPe}} \tag{25}$$

$$\Delta T = \frac{P_{HPth}}{c_w \dot{m}_w} \tag{26}$$

$$T_{HPout} = T_{HPin} + \Delta T \tag{27}$$

$$T_{HPout} = T_{HPin} + \psi \frac{P_{HPe} \cdot 0.5(T_{HPout} + T_{HPin}) + 273.15}{c_w \dot{m}_w \cdot 0.5(T_{HPout} + T_{HPin}) - T_a} \tag{28}$$

The HP is strategically connected in series with the return piping, near the main thermal plant. Its primary function is to compensate for the limited thermal power provided by the EG recovery system by increasing the temperature of the return water. The HP is driven by a variable speed Induction Motor (IM), which is controlled using direct torque control technology. To regulate the thermal power generated by the HP, a temperature hysteresis control is employed, which turns the HP on or off to prevent the undesired evaporation of water during light thermal loading conditions. However, for ancillary services, the frequency droop control of the IM driving the HP is used here to directly control its speed, demonstrating through dynamic studies that thermal comfort is not affected by temporary HP thermal power reductions.

2.5. KLFN community example

This subsection presents the methodology employed to estimate the total thermal demand in the KLFN community, and discusses the feasibility and challenges of deploying a DHN to properly supply the community's thermal needs, based on the relevant DHN models and controls presented in the previous sections.

2.5.1. Thermal demand estimation

By using the household's thermal model provided in [22] for a typical North American house, the thermal demand of the community homes and buildings can be estimated based on the specific area considered. A normalization technique can then be used to estimate the thermal load for each residential house in the KLFN community, where there are 215 residential homes. There are also 10 additional community and commercial buildings, which include the school, police station, band office, nursing center, and church, with each of these structures

being modeled independently as a separate consumer group using the same household thermal dynamic model discussed in Section 2.1, and based on their respective areas, heights, and usage patterns. A water treatment plant and sewage plant, where heating is only provided to the control rooms, are also part of the community buildings. A large grocery store and a hotel form the commercial demand.

The thermal power demand of a building can be estimated using the following equation [34]:

$$P_{Hth} = AS_H \overline{P}_{Hth} \tag{29}$$

Based on the SRLS, a thermal peak power of around 16.4 kW is necessary to fulfill the heating requirements of a 196 m^2 area. This calculation takes into account a minimum ambient temperature range of −38 °C over a 24-h time interval in January, according to [35], with a maximum indoor setpoint temperature of 25 °C. The residential houses in the KLFN community are categorized as either single-detached, semi-detached, or row houses, as per [36]. These house structures adhere to the standard Canadian house design [22]. The normalized area A for each house can be obtained using Google Earth to determine the areas of the 215 houses and the other 10 community and commercial buildings, which allows to calculate the thermal demand of the DHN.

The design of the piping routing plays a critical role in the establishment of a radial DHN. In this study, the THERMOS program has been utilized to generate the optimal routing, determine the appropriate pipe diameters, and calculate the actual length of the pipelines specific to the particular case being studied [37]. To estimate the maximum thermal power demand in the KLFN community for piping purposes, the following steps are used:

1. Run the SRLS for a standard Canadian household, considering the worst expected weather conditions, neglecting solar thermal power and internally generated thermal power.
2. Assign the maximum required thermal demand for an individual household and apply the area normalization procedure to obtain the required thermal demand for each of the 215 houses, as well as community and commercial buildings.
3. Utilize THERMOS to estimate the piping routing requirements.

2.5.2. Thermal demand grouping

Simulating all residential houses in a potential DHN is time-consuming and computationally demanding. To reduce simulation time, the model assumes groupings of nearby thermal loads, treating them as a single load. This methodology significantly reduces simulation time while maintaining accuracy, based on pipe length limitations and the DHN characteristics. Thus, the grouping of houses is limited to a distance of 150 m along the radial DHN, ignoring the temperature drop within this distance. No grouping is considered for pipeline lengths less than 50 m to minimize the number of groups. Furthermore, due to the faster response of the mass flow rate to internal or external variations compared to the radiator return temperature, the thermal power of a building can be assumed to be directly proportional to the mass flow rate.

2.5.3. Piping routing design

The pipeline system under consideration consists of a double-way routing and comprises several layers, as depicted in Fig. 2. These layers include: (1) a Carbon steel layer, which is the first layer of the pipeline and serves as the structural component; (2) a Polyurethane insulation layer, which is composed of Polyurethane insulation material with a very low thermal conductivity to minimize heat transfer and reduce heat loss from the pipeline; and (3) a Polyisocyanurate insulation layer, which also presents low thermal conductivity. All these layers are buried underground at a depth denoted by Z to protect the pipeline and insulation layers from external environmental conditions and further minimize heat loss. Table 1 presents the key thermal properties and parameters of the materials used in the pipeline insulating system.

The following issues need to be considered in the design of the DHN piping network for the KLFN community:

Table 1
Piping network design parameters.

Parameter	Value
Carbon steel density	7843 kg/m^3
Carbon steel specific heat capacity	434 J/kg °C
Carbon steel thermal conductivity	45 W/m °C
First-insulator density	30 kg/m^3
First-insulator specific heat capacity	1500 J/kg °C
First-insulator thermal conductivity	0.02 W/m °C
Second-insulator density	32 kg/m^3
Second-insulator specific heat capacity	1400 J/kg °C
Second-insulator thermal conductivity	0.02 W/m °C
Soil thermal conductivity	0.38 W/m °C
Water thermal conductivity	0.64 W/m °C
Pipeline burying depth	0.6 m

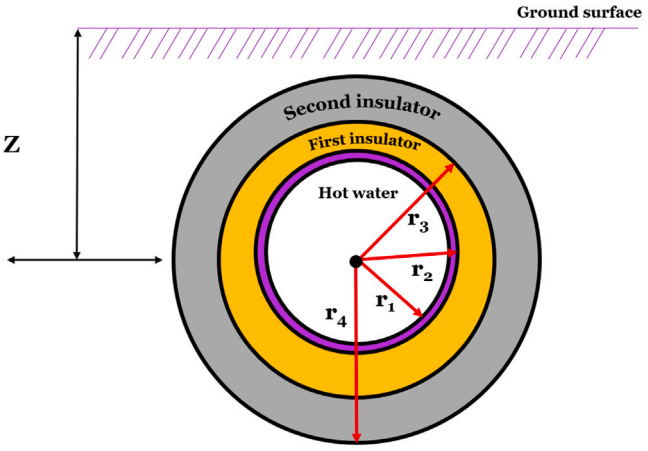


Fig. 2. Cross-sectional design of a DHN pipeline.

- The linear heat density in the community is significantly lower compared to most typical DHNs. This results in a high ratio between piping heat loss and thermal demand.
- The soil properties in KLFN impose limitations on burying depth and the feasibility of excavation, since the considered area is predominantly covered by up to 4 m of glacial boulder till, overlaid by 20–30 m of fine sand and clay [38]. These soil conditions complicate the civil engineering works, thus increasing deployment costs.
- The community experiences harsh weather conditions, with temperatures dropping as low as −38 °C during the Winter season. These extreme low temperatures further increase heat loss in the pipes.
- The main thermal plant is located approximately 1.65 km away from the starting point of the thermal demand. This results in increased heat losses and affects the QOS.

To minimize the excessive piping heat loss in the KLFN community, the following needs to be considered:

- Due to the composition of the soil, increasing the burying depth is not feasible. Thus, the maximum burying depth considered is 0.6 m, as per recommended standards [39].
- Modern insulation materials with low thermal conductivity, such as Polyurethane or Polyisocyanurate, are used to increase pipeline radial thermal resistance and reduce heat loss transfer.
- To minimize soil thermal conductivity, artificial soil such as mixed sandy loam can be used [40]. Although this approach may have a high initial cost, it is necessary to reduce the excessive piping heat loss. Moreover, by utilizing EG from diesel engines, the CHP system efficiency can be improved, potentially offsetting initial costs over time. This cleaner heating source decreases

Table 2
Pipeline layers' diametrical ratios for Fig. 2 in KLFN.

r_2/r_1	r_3/r_2	r_4/r_3	r_4/r_1
1.1	1.364	1.333	2

Table 3
EG recovery system data for different DG loadings.

DG loading (%)	100	75	50	25
EG temperature (°C)	524.0	524.0	457.5	452.1
EG flow (kg/s)	5.742	5.742	5.278	4.784
Heat rejection (kW)	1202	1202	1038	933

Table 4
KLFN Thermostat temperature setpoints.

Building	Time intervals		Setpoint
	From	To	
Residential	9 AM	5 PM	18 °C
	6 PM	8 AM	25 °C
Commercial	6 AM	10 PM	25 °C
	11 PM	5 AM	18 °C
Community	8 AM	5 PM	25 °C
	6 PM	7 AM	18 °C

the KLFN community's reliance on oil, reducing high carbon emissions and pollution, and enhances the EPN reliability by taking advantage of the DHN's thermal inertia. These benefits may justify the high initial cost of the IEHS in remote communities.

These considerations yield the diametrical ratios presented in Table 2 for different layers of carbon steel and insulation materials relative to the original inner pipe diameter, ensuring efficient heat transfer and minimizing heat loss.

2.5.4. Waste heat recovery system

The assumed waste heat recovery system employs an HX to extract thermal power from the EG of KLFN community diesel engines through water heating. The energy collected by the recovery system is modeled using tabular data from Caterpillar generators [41], with Table 3 illustrating the EG recovery system data for different DG loadings. This data varies with DG electrical loading conditions. The EG recovery system's energy consumption is minimal, primarily involving the operation of a control valve that regulates the EG mass flow rate, and thus its energy consumption is negligible compared to the energy collected, resulting in a rather large efficient factor.

2.5.5. Simulation results

This subsection presents some relevant results for the designed DHN of the KLFN community, with the dynamic components of the KLFN's DHN being modeled with equations (1)–(28) in Matlab/Simulink, with a fixed discrete solver and a time step of 0.278 ms. This time step was chosen because Matlab/Simulink simulation must be run in seconds and not hours, which are the time constants of the DHN model; hence, one can convert the DHN time-based signals from seconds to hours as follows: $0.278\ \text{ms} \times 3600 = 1\ \text{s} \equiv 1\ \text{h}$. The setpoint temperatures range from 18 °C to 25 °C, at different times depending on the building topology. Table 4 illustrates the thermostat setpoints used for different KLFN community structures.

The presented results correspond to January 2, 2020, for 24 h and considering solar irradiance data from [35]. Fig. 3(a) illustrates the variation in temperature setpoints for a consumer group situated at the distant end of the DHN, which has the largest temperature drop in the system. Note that when the temperature setpoint is low, the space temperatures do not decrease rapidly due to the existing solar thermal power and the thermal inertia of the spaces. The temperature

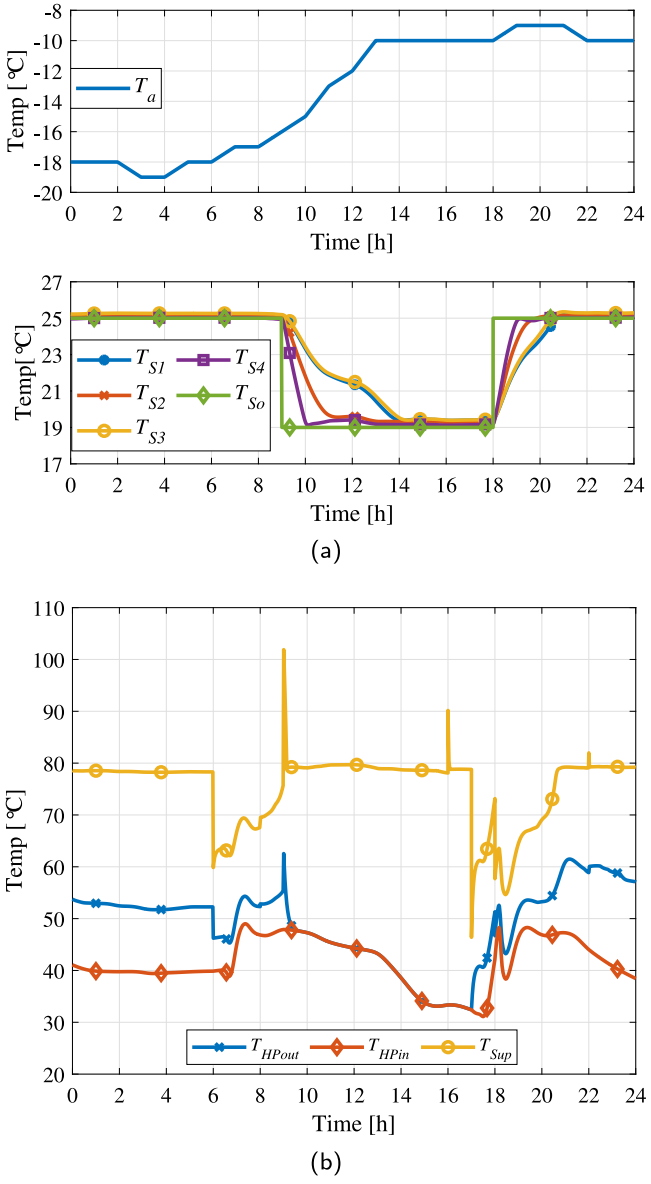


Fig. 3. (a) Ambient temperature and temperature response of the thermal group located at the far end of the DHN, and (b) temperature response of the thermal power plant and the HP.

response illustrates the temperature of each space within the four areas considered for a household. Observe that the modeled TRVs effectively track the temperature setpoints under the given ambient temperature conditions, ensuring satisfactory temperature regulation within the different spaces.

Fig. 3(b) depicts the regulated supply temperature T_{Sup} and water temperatures T_{HPin} and T_{HPout} of the HP. Since this device assists in preheating the return water when the thermal demand exceeds the capability of the EG heat recovery system, to ensure satisfactory QOS and accurate tracking of the temperature setpoint, the outlet temperature of the HP increases when it is active.

The required on/off HP operation is performed once every several hours, taking into account the high mechanical inertia of the IM driving the HP. Fig. 4 illustrates the dynamics of thermal power demand, EG recovered power, piping heat loss, and HP-generated power. Note that the heat demand increases with increasing temperature setpoint and decreases with decreasing setpoint. Similarly, the generated thermal

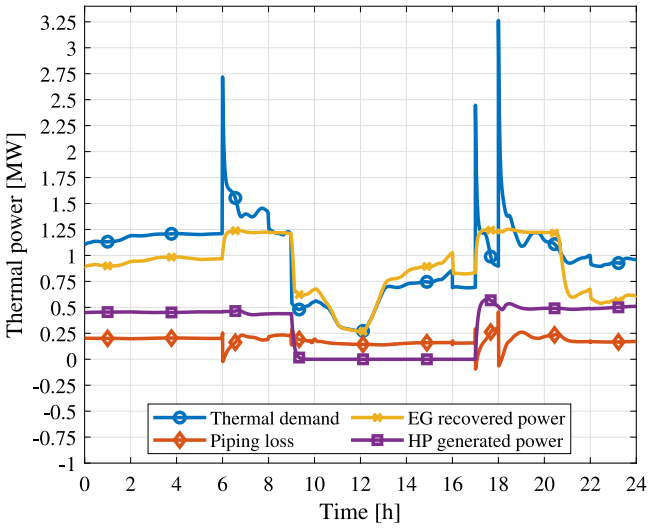


Fig. 4. Thermal power demand, EG recovered power, piping heat loss, and HP-generated power.

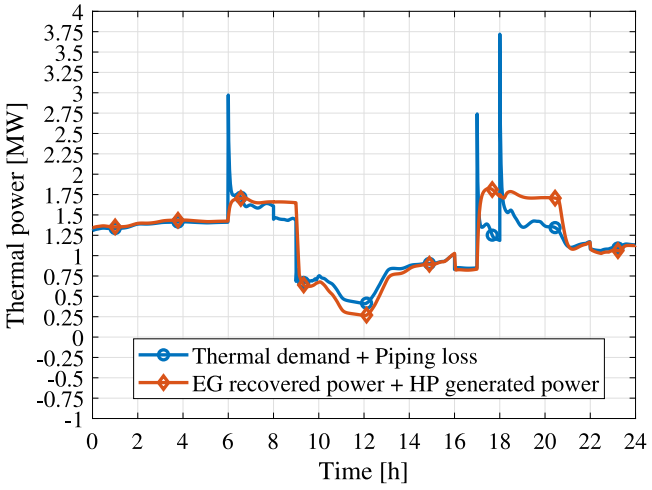


Fig. 5. Heat balance between the thermal supply and demand of the KLFN DHN.

power is proportional to the thermal demand, but it does not necessarily balance the heat demand instantaneously, as expected. Observe that the piping thermal losses under steady-state conditions do not exceed 20% of the thermal demand due to the use of low thermal conductivity insulators within the system, which is necessary in remote communities for the considered pipelines [42].

The fluctuations in the supply temperature in Fig. 3(b) and the thermal demand in Fig. 4 are due to the dynamic behavior of the DHN customers. For instance, at 9 h in Fig. 3(b), a decrease in setpoint temperatures by DHN consumers causes radiator valves to lower the hot water mass flow rate, significantly reducing the total thermal demand. This change is rapid, as radiator valves react within seconds, and requires a reduction in generated power, as depicted in Fig. 4 at 9 h. Due to the time lag in the EG valve response, there is a temporary excess in thermal energy storage, which heats the supply water and increases its temperature. The same principle applies when thermal demand increases, leading to supply temperature fluctuations due to the time lag in adjusting the generated power. This lag in the EG valve controller is imposed to prevent the hot-water supply from boiling, which could cause pressure problems in the DHN piping system.

The heat balance between the thermal demand plus piping losses and the EG recovered power plus HP generated power is shown in Fig. 5, showing that there are periods when the heat supply is either less than or greater than the heat load demand, with this deviation being managed through the thermal inertia of the DHN. For example, at 6 h in Fig. 4, the thermal demand exceeds the supply, with the deficit being compensated by drawing thermal power from the DHN stored thermal energy, resulting in a decrease in the supply temperature as shown in Fig. 3(b). Conversely, at 9 h, when the supply exceeds the demand, the excess energy is stored, increasing the supply temperature. The slight time lag between the net stored energy and the supply temperature variation observed is compensated by the DHN thermal inertia acting as a buffer, smoothing out discrepancies between supply and demand, maintaining stability in supply temperature, and ensuring continuous and reliable heat delivery. To control thermal heat generation, both the EG recovery system and the HP are controlled to avoid undesirable spikes. This is achieved through an exhaust gas valve control for the EG recovery system and the direct torque load control of the HP, as previously discussed.

The aforementioned results demonstrate the feasibility of deploying a DHN in an actual remote community in the North. It is shown for the first time through detailed dynamic studies that the community thermal needs can be properly supplied by a DHN that takes advantage of the waste heat of DGs in the community's EPN. These results further strengthening the case for such DHN deployment in remote communities, which have been demonstrated through economic analyses based on static DHNs model. However, it is also shown that to accomplish this, there are challenges that need to be addressed with respect to DHN proper design and deployment, which may have a significant impact on the potential deployment of DHNs in these communities, as it has been suspected but it is now demonstrated in this paper through detailed dynamic modeling and studies.

3. EPN model

Due to space constraints, this section describes briefly the traditional dynamic models considered for EPNs in remote microgrids, and focuses on discussing the results of applying them to study the IEHS for the KLFN community. It also demonstrates the use of demand response control in the DHN HP for EPN frequency regulation to facilitate the integration of RES in remote microgrids.

3.1. Isolated microgrid dynamic model

3.1.1. Diesel generator

Synchronous DGs are widely used in remote microgrids as dispatchable grid-forming resources to support the system frequency. In this work, the Simscape Electrical library is utilized for accurate DG dynamic modeling, including all required controls [43]. The synchronous machine model simulates the behavior of an alternator and can be adjusted to fit the specific parameters of microgrid generators. Cascading blocks are used to represent the governor droop for frequency control. The automatic voltage regulator model ensures that the terminal voltage is maintained at the specified nominal voltage levels.

3.1.2. Wind generators

The Wind Generators (WGs) modeled here are based on full Voltage Source Converter (VSC) interfaces. The VSC model utilized for the WGs, along with its controls, is described in detail in [44].

3.1.3. PV panels

The PV array block considered here contains PV modules arranged in parallel and series strings, with a "perturb and observe" control that adjusts the panel's voltage and current to track the maximum power point. This control algorithm optimizes power generation output by adapting to changing conditions as explained in detail in [45].

Table 5
HP IM drive parameters.

Parameter	Value
P_{HPo}	250 kW
k_c	0.04354 kW s^3
$\Delta\omega_{HP}$	125.664 rad/s^2
k_{HP}	60 p.u.
k_p	10 p.u.
k_i	100 p.u.

Table 6
KLFN Generator ratings.

Generator type	Rating
DG1	1500 KW
DG2	1000 KW
DG3	600 KW
WG	60 KW
Exist. PV	10 KW
Added PV	250 KW

3.1.4. Electric loads

A constant impedance Z, current I, and power P load model is considered in the presented studies, which properly reflects the voltage sensitivity of microgrid loads [44].

3.1.5. Heat pump ancillary services

The DHN has a longer time response compared to the EPN due to its significant thermal inertia. This unique characteristic allows the DHN to play an important role in regulating the frequency of the EPN. Thus, for primary frequency control, the electrical demand of the HP can be adjusted for a specific duration, allowing to provide frequency regulation, while maintaining the desired DHN QOS. This is accomplished here using a frequency droop control to manage the speed of the three-phase variable speed IM that controls the thermal power generated by the HP, which can be modeled with the following equations that account for the compressor load torque applied to the HP's IM shaft:

$$\omega_{HPo} = P_{HPo} + k_{HP}\Delta f \tag{30}$$

$$\Delta f = f - f_o \tag{31}$$

$$\tau_{HP} = k_c \omega_{HPo}^2 \tag{32}$$

Droop control allows the HP IM to improve the performance of the EPN frequency response compared to solely applying droop control to the DG units. Table 5 depicts the main parameters used to represent the HP IM drive model, including the maximum change in angular velocity $\Delta\omega_{HP}$.

To fully leverage the high thermal inertia of the DHN, it is proposed here to implement a secondary frequency control strategy to rapidly mitigate steady-state frequency deviations within seconds, thereby eliminating the need to wait for approximately 15 min for DG redispatch, which is the usual dispatch rate of microgrid energy management system [9]. Thus, secondary frequency control is implemented here on the HP's IM drives utilizing an anti-wind Proportional–Integral controller. This controller is employed to adapt the HP shaft power reference, based on the following equation:

$$P_{HPo} = K_p \Delta f(t) + K_i \int \Delta f(t) dt \tag{33}$$

The HP demand response used here for frequency regulation purposes has a negative impact on the HP thermal power, which affects the performance of the DHN. In this context, it is important to study the temperature changes in the community to evaluate the impact of the HP thermal power reduction on the DHN dynamics, considering the typical 15 min dispatch of the EG heat source, which is within the dynamic time constants of the DHN. This issue cannot properly captured in existing studies based on DHN static models.

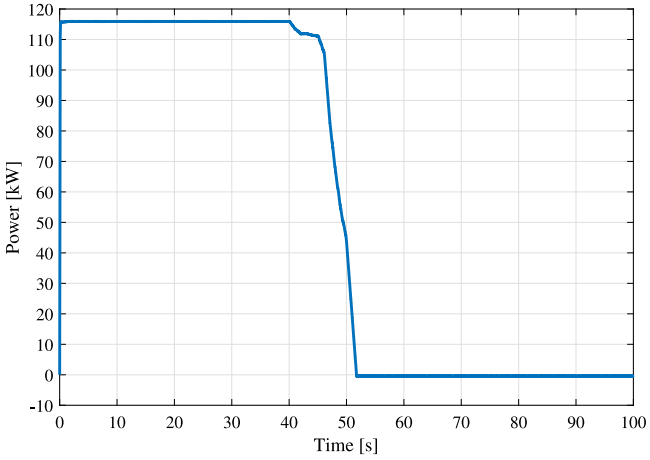


Fig. 6. Power fluctuation of PV panels, with a sudden trip at about 50 s.

3.2. KLFN community example

3.2.1. EPN description

Each dynamic component of the KLFN's EPN system is modeled using Simscape in Matlab/Simulink, with a fixed discrete solver and a time step of 0.1 ms. The simulations are based on measured data from existing electrical sources and loads, collected at the KLFN community during 2014 and 2015 to study the deployment of additional RES for the EPN [46]. Thus, there are three 1500 kW, 1000 kW, and 600 kW DG units. As per the utility's dispatch rules, only one unit operates at a time. Additionally, there is a 10 kW roof-top PV panel and 4 wind turbines totaling 60 kW (three 10 kW single phase converter-interfaced units and one 30 kW direct-connected unit), which are modeled here as a single VSC-interfaced unit, to represent WG systems currently being deployed in isolated microgrids. A 250 kW PV array is also considered to study the impact of RES power fluctuations on the performance of the EPN, as discussed in [47].

Fig. 6 shows the PV power fluctuations observed from the modeled 250 kW PV panel, based on scaled real measured data of the existing 10 kW PV panel over a 100 s time window. A sudden loss of PV generation at about 50 s due to a grid contingency is assumed to test the IEHS performance for a significant EPN contingency.

The demand of the commercial and community buildings are represented using measured data collected for the various existing facilities, and the total residential demand is calculated by subtracting the demands of the commercial and community buildings from the measured total generation, realistically assuming minimal losses in the microgrid feeders. A 24.7% unbalance condition is considered, as commonly observed during Winter months in the KLFN microgrid [46]. During the simulation for January 2, 2020, considered in the DHN studies, the electrical load is assumed initially to be 523.6 kW, with the demand gradually increasing and peaking roughly at 900 kW, excluding the HP power demand. The 1000 kW DG unit is assumed to be supplying the electrical load needs.

Table 6 presents the nominal power of various generation sources in the community. Additionally, Table 7 presents the power ratings for different types of loads considered in the simulation. These loads are modeled as 60% constant Z, 30% I current, and 10% constant P.

Fig. 7 shows the KLFN's IEHS structure, depicting the KLFN potential DHN described in Section 2.5, illustrating 55 thermal load groups corresponding to 215 residential houses along with the 10 community and commercial buildings. This figure shows the interconnections between the EPN and the DHN.

In the KLFN IEHS, both the DG and the HP IM present frequency droop controls with opposite slopes, as shown in Fig. 8. The compressor load torque in the IM drive is modeled with (32).

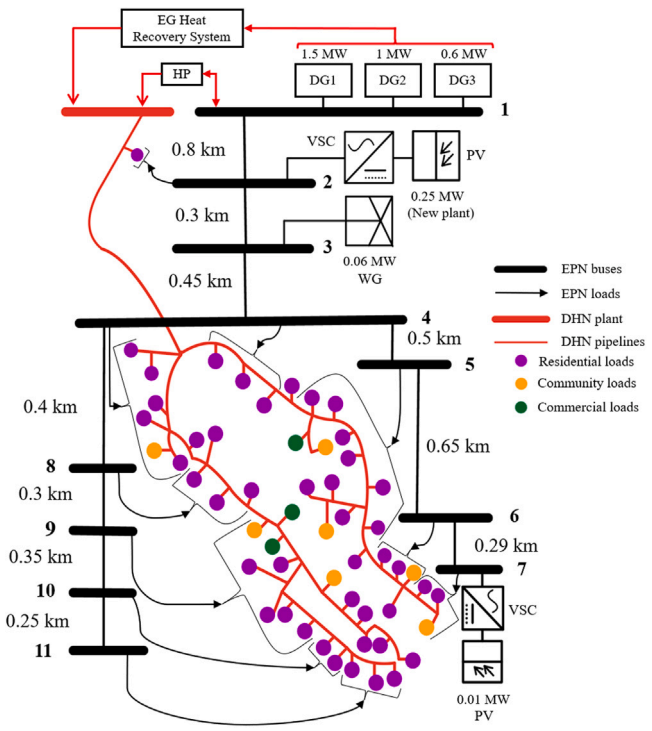


Fig. 7. KLFN Community IEHS.

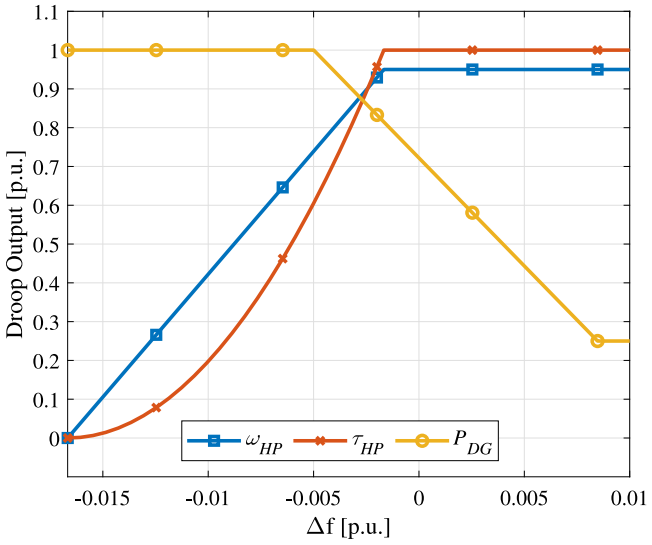


Fig. 8. Droop control for DGs and HP IM.

Table 7
KLFN Load types and powers.

Load type	Min.	Max.
Police station	8.07 kW	13.6 KW
School	11.03 kW	18.6 KW
Sewage plant	3.56 kW	6 KW
Water treatment plant	19.4 kW	32.7 KW
Nursing station	12.1 kW	20.4 KW
Grocery store	37.55 kW	63.3 KW
Residential	431.84 kW	760.8 KW

3.2.2. Simulation results

The frequency response for KLFN EPN is illustrated in Fig. 9 for the 100 s studied window for four distinct case studies:

- Case 1 represents the EPN operating independently without the DHN, solely supplying the base electrical load of 688 kW.
- Case 2 examines the IEHS without HP demand management.
- Case 3 studies the IEHS with HP droop control.
- Case 4 correspond to the IEHS with HP secondary frequency control capability.

Observe in Fig. 9 that the electrical load stays close to 688 kW (excluding HP power consumption for Case 1), since the voltage at the load buses does not change significantly, consistent with [47]. Note the initial frequency variations due to the system components' startup, notably the DG, the WG, and the HP's IM, followed by a steady frequency for roughly 40 s, given the fixed PV output power during this period. Subsequently, there is a change in solar irradiance probably due to cloud movement followed by loss of PV generation at about 50 s, resulting in the frequency dropping to 59.84 Hz for Cases 1 and 2. During this period, only the DG droop control is responsible for regulating the frequency in these two cases, while the demand from the HP motor remains constant. In contrast, with the HP droop control, Case 3 shows a faster frequency response and reduced frequency deviation compared to Cases 1 and 2, with the frequency stabilizing at 59.89 Hz. The best frequency response is achieved in Case 4 by implementing secondary frequency control, which restores the frequency to 60 Hz within 15 s, without relying on the 15 min DG redispatch process.

Fig. 10 presents the power output from the DG unit for Case 3, which remain fixed at 825 kW to supply the base EPN and DHN HP loads, as per the required dispatch rules at KLFN [47]. Note that the power and shaft speed of the HP change with the frequency due to the HP secondary frequency control.

The variations in electric power generation due to the loss of PV generation significantly influences the thermal power supplied to the DHN, primarily due to the reduction in HP shaft power interacting with the EPN frequency variations, as depicted in Fig. 11. Following the loss of PV generation, a 15 min monitoring period of HP and DG powers is used to assess the worst-case scenario before a subsequent DG redispatching, reasonably assuming constant thermal power demand. In contrast, the base electric load undergoes a ramp variation from 688 kW to 753 kW, based on measured data for the KLFN community. Despite these EPN generation and load fluctuations, DG power remains relatively constant at 825 kW, while HP shaft power notably decreases from 242 kW to 87 kW to compensate for both the loss of PV generation and the increase in the base load during the 15 min interval to mitigate EPN steady-state frequency deviations. At the same time, HP thermal generation decreases from 490 kW to 200 kW, indicating a significant loss in thermal power generation that impacts the DHN supplied thermal power. Additionally, Fig. 11 illustrates HP's COP variations, highlighting its nonlinear variation, which directly depends on HP thermal and electrical power values.

As shown in Fig. 10, the electrical system is being simulated with seconds resolution, whereas the thermal system is simulated with min resolution, as shown in Fig. 11. This is possible due to the IEHS electrical and heating systems having different time constants, since for example, the thermal inertia of the HP is much higher than its mechanical inertia, thus allowing the computationally efficient co-simulation of the two systems with different time scales, using fractions of a second for the electrical system and fractions of a minute for the thermal system, without significant simulation errors. The use of the shorter electrical system time intervals to simulate both systems would require extensive computation time, without significant changes in the results.

It is important to highlight that in the 15 min interval shown in Fig. 11, the load varies gradually, as per actual measurements at the KLFN community [47], while the DG power remains basically fixed, since this is only re-dispatched every 15 min through a typical energy management system. The figure shows that the DG governor's impact on the generator power output is small, since the HP regulates the frequency in this case, as illustrated in Fig. 10.

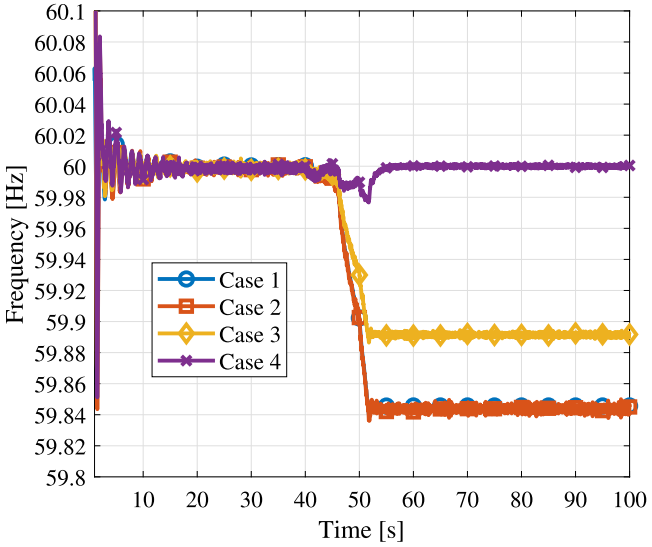


Fig. 9. Comparison of frequency response with and without DHN and HP droop control.

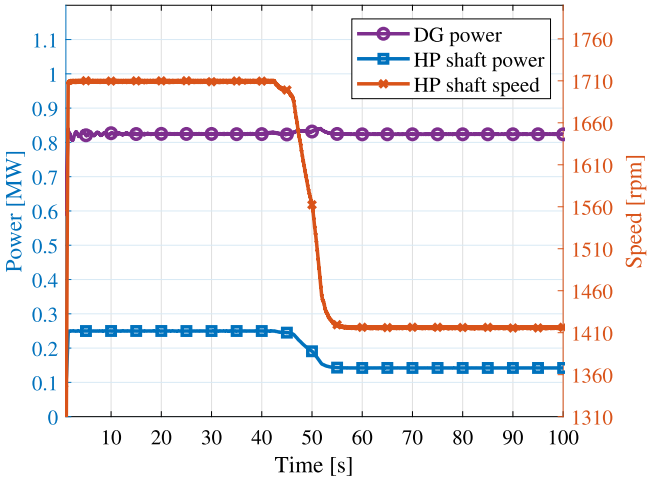


Fig. 10. Generator power, HP shaft power, and shaft speed with frequency changes.

To examine the impact of HP thermal power reduction due to droop and secondary frequency controls, Fig. 12 depicts the DHN temperature dynamics. Observe that due to the high thermal inertia of the DHN, noticeable change on building temperatures would require a considerable amount of time, as depicted in Fig. 12. This figure illustrates the various building spaces and setpoint temperatures for the consumer group situated at the distant end of the DHN for the studied 15 min timeframe. Thus, the minimal heating requirements are met without disrupting consumer QOS, assuming no heat load service interruptions, with only a 0.15 °C temperature drop in 15 min after the HP thermal power reduction. This indicates that it would take several hours for DHN customers to notice any significant impact from the reduced thermal power generation in the HP. Furthermore, after 15 min, these slight temperature changes would be corrected with the DG unit re-dispatch that allows resuming the HP normal operation.

When the EG thermal power generated is sufficient to supply the KLFN thermal demand, the HP would not be needed and hence would be turned off. Consequently, secondary frequency control cannot be provided using the HP, with the DG unit having to deliver this regulation service during the usual 15 min DG redispatch intervals, as it is now the case in existing remote EPNs, which is costlier compared to utilizing the DHN thermal inertia for this purpose.

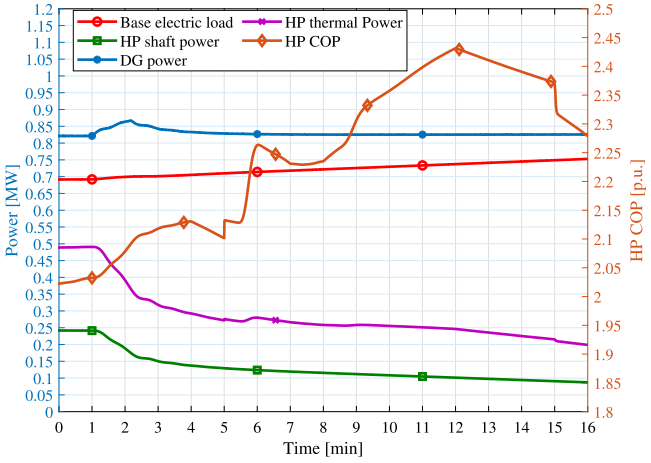


Fig. 11. Generator power, HP shaft and thermal powers, base electric load, and HP's COP.

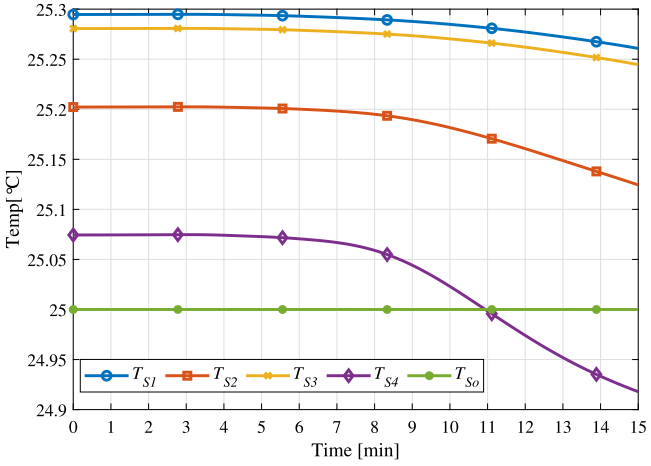


Fig. 12. Temperature response of the thermal group located at the far end of the DHN after HP thermal power reduction imposed by the secondary frequency control.

3.2.3. Electric thermal storage heating

To further highlight the effectiveness of the potential DHN in the KLFN community, this section discusses the case where all thermal demand in KLFN community is met by individual ETS units currently deployed in some remote communities, comparing the EPN performance with respect to the IEHS results.

To estimate the electric power demand required to fulfill the thermal demand of the community with ETS units, the SRLS tool was used. Thus, Fig. 13 illustrates the building heating control for the ETS units used in the SRLS to represent the thermal dynamics of a household. The model takes into account external ambient temperature and the thermal power generated by the ETS units to maintain the household space temperatures at a specified setpoint by adjusting the discharge resistance R_{disch}, which reflects the variable speed of the ETS unit's heat distribution fan. In this case, it is assumed that all ETS units utilized in KLFN community have an overall efficiency of 95%. Further details of the dynamic modeling and control of the ETS unit are available in [48,49], and [50].

To ensure an equitable comparison between IEHS with DHN and with ETS units for ancillary services provision, demand management is also applied to the ETS units, based on the approach outlined in [51], which is implemented here using the following equations:

$$f_{DR} = \frac{1}{1 + e^{k_{DR1}(\Delta f + k_{DR2})}} - \frac{1}{2} \tag{34}$$

Table 8
ETS demand response control parameters.

Parameter	Value
k_{DR1}	−600 p.u.
k_{DR2}	−0.02 p.u.
k_{DR3}	100 p.u.

$$\frac{dP_{DR1}}{dt} = k_{DR3} f_{DR} \overline{P}_{DR} - P_{DR1} \tag{35}$$

$$P_{DR2} = \min\left(|\mathbf{P_{DR}} - P_{DR1}\mathbb{1}|\right) \tag{36}$$

where the control function f_{DR}, based on sigmoid function due to its smooth, non-linear, saturating behavior, and ease of adjustment, effectively generates the desired demand response P_{DR1} based on the frequency deviation Δf, with constants k_{DR1}, k_{DR2}, k_{DR3}, and $\overline{P}_{DR}$ defined in the Nomenclature. P_{DR1} is then compared with $\mathbf{P_{DR}}$, which signifies the vector encompassing all the potential on/off combinations of ETS power consumption of 55 groups in the KLFN community. The value closest to P_{DR1} among the elements of $\mathbf{P_{DR}}$ defines the ETS load combination selected to generate the actual actuating demand response P_{DR2}. Table 8 presents the parameter values used in (34)–(36) to model the demand response control of the ETS units, which determine their response for primary frequency control.

Fig. 14 depicts the thermal demand of the community with a DHN vis-à-vis the ETS units. Note the need for a minimum 1.8 MW power capacity to fulfill the required heat demand using only ETS units. Considering a peak electrical load of 0.9 MW for the studied day results in a total demand of 2.7 MW for both electrical and thermal loads. Hence, two DG units would need to be dispatched, which is not the usual dispatch strategy in remote Ontario communities [52].

Two additional case studies are added to the previously discussed four cases:

- Case 5 correspond to the EPN and ETS heating units without ETS demand response control.
- Case 6 incorporates the EPN and ETS heating units with ETS demand response control.

For these cases, the total electrical load of the EPN is 2,488 kW, being supplied by the DG units DG1 and DG2 which corresponds to 688 kW of base electric load, as in the EPN+DHN simulations, and 1800 kW of demand from the ETS units. The two generators have droop control, sharing the power changes proportionally to their capacity.

Under the same fluctuations in PV panel power discussed in Fig. 6, Fig. 15 depicts the frequency responses for the IEHS and the EPN equipped with ETS units, for the same 100 s time window utilized before. Observe that in ETS Cases 5 and 6, the frequency deviation is lower compared to the droop control Cases 1, 2, and 3. This can be attributed to the presence of two generators, which effectively distribute PV fluctuations. Note that distributed ETS demand response enhances the primary frequency control of the EPN compared to the centralized HP-based control. However, this requires a more complex distributed approach, with more significant control and communication requirements than the centralized HP-based frequency regulation technique. Furthermore, the proposed ETS frequency regulation control presents significant uncertainties associated with the individual ETS power availability. Finally, the proposed HP demand response for frequency regulation facilitates the implementation of a secondary frequency control.

From the presented results, the advantage of using a DHN versus ETS units to supply the community thermal loads is clear. Thus, first, emissions would significantly increase with the ETS units, as more DG units would need to be dispatched, and the DG exhaust thermal power not being utilized. Second, the DHN would allow a better integration of variable RES through the ready utilization of its significant thermal storage capacity via HP frequency droop control. Finally, the IEHS featuring HP droop control and secondary frequency control would be preferable over the use of ETS units due to a simpler communication network and control requirements, plus smoother and less uncertain HP speed control compared to ETS demand response switching.

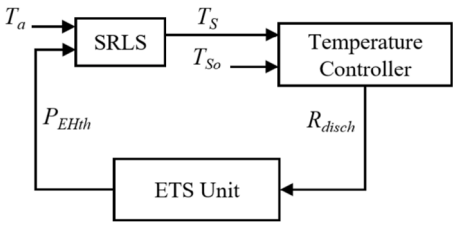


Fig. 13. Schematic of building heating with ETS unit.

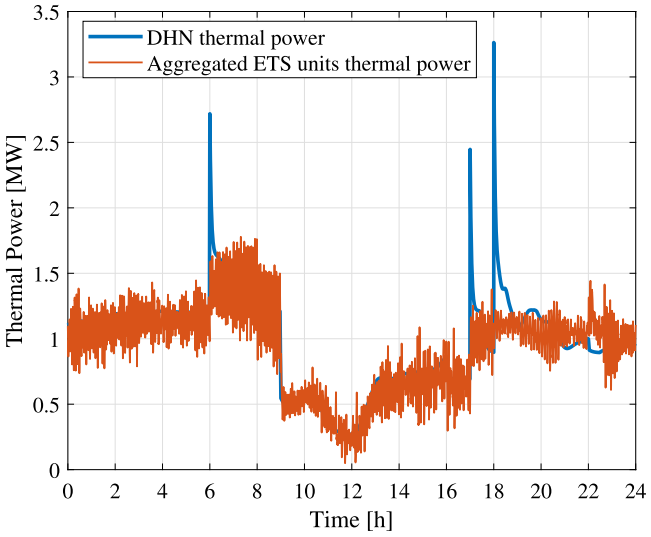


Fig. 14. Comparison between DHN and ETS units for thermal demand provision.

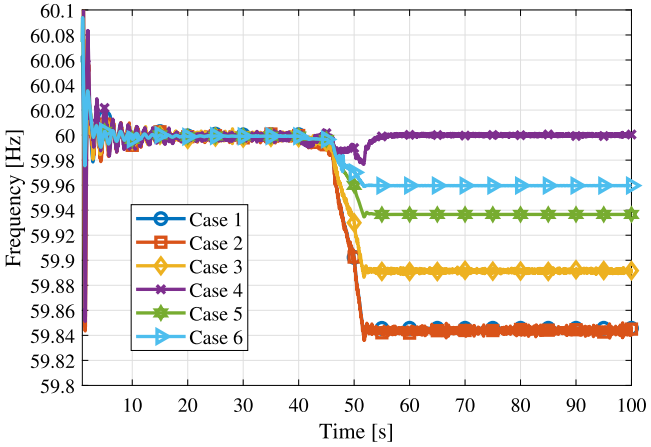


Fig. 15. Comparison of frequency response between IEHS and EPN with ETS units.

3.2.4. HP and ETS frequency control comparison

This section compares the performance of the demand response centralized control of ETS units and the centralized HP droop control for primary frequency control in the KLFN EPN. To accomplish this, a step increase in base load from 686 kW to 825 kW at 50 s is studied here, with the power output from the RESs remaining constant. Fig. 16(a) shows that both controllers react by adjusting their demand

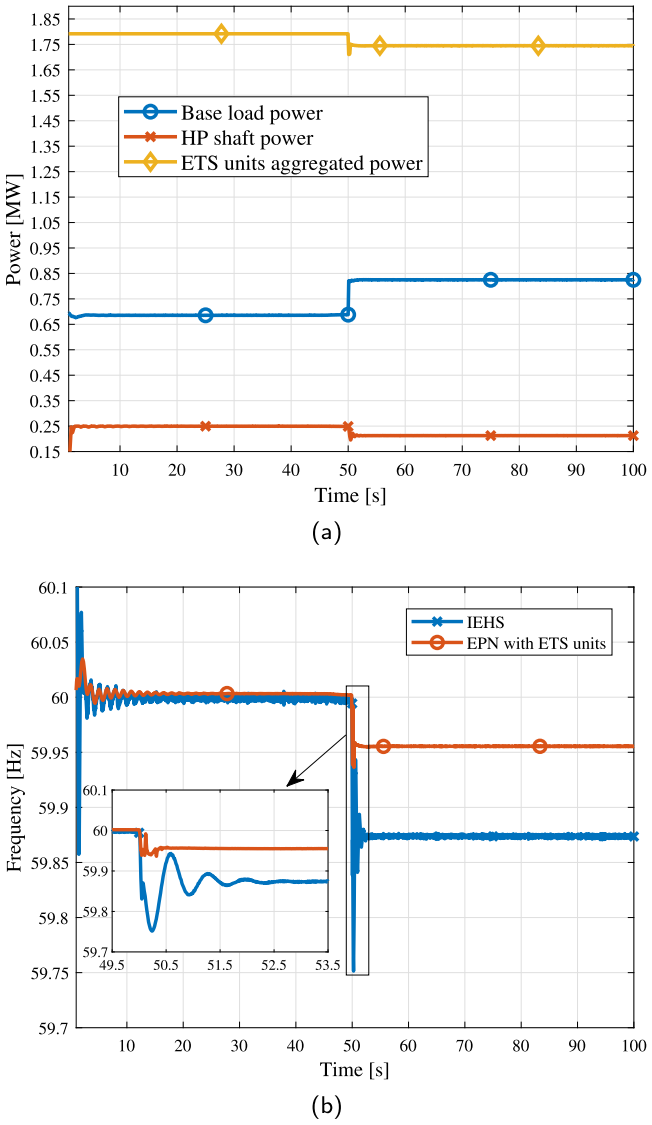


Fig. 16. Comparison of primary frequency control response between IEHS and EPN with ETS units for a step load increase: (a) electrical power and (b) frequency.

to maintain adequate primary frequency control, with the ETS units' demand decreasing from 1792 kW to 1745 kW and the HP shaft power decreasing from 250 kW to 213 kW. However, Fig. 16(b) demonstrates that the ETS demand response control is faster than the centralized HP droop control. This is due to the overall mechanical inertia of the HP and its droop control, which allow the IM speed change to regulate the frequency with a maximum rate of speed change of ±1200 RPM/s to realize a smooth speed control, which causes latency in the HP shaft power's response, thus affecting frequency control. On the other hand, the centralized ETS control utilizes multiple ETS units across the community, resulting in a faster control response through the on/off operation of designated ETS units. As shown in Fig. 16(b), the time difference between both controllers before reaching a stable frequency is roughly 2 s, illustrating the faster ETS demand response for primary frequency control.

3.2.5. IEHS frequency control for overlapping RES and load fluctuations

To further evaluate the capability of the DHN for providing effective secondary frequency control in remote microgrids, the KLFN IEHS is tested under an overlapping RES dips and a sudden load increase. Thus, as depicted in Fig. 17, the PV power fluctuations are the same

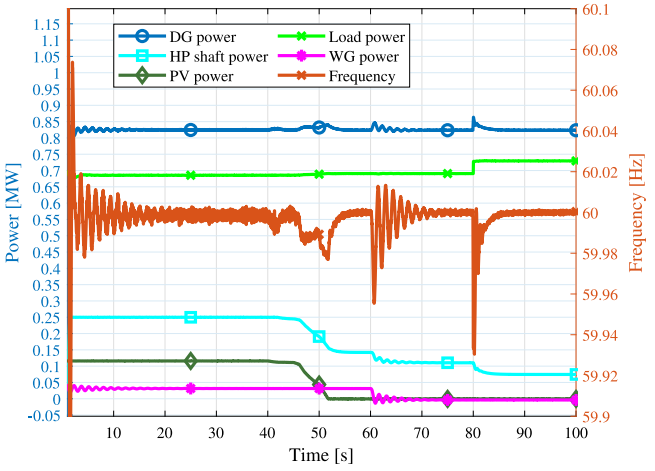


Fig. 17. IEHS secondary frequency control under overlapping RES and load fluctuations.

as those shown in Fig. 6, but now an additional sudden loss of 31 kW of WG power is assumed to take place at 60 s. Furthermore, a load step from 688 kW to 730 kW at 80 s is introduced. As expected, observe that the HP power decreases its power to help maintain a stable frequency at 60 Hz through its primary and secondary frequency controls. Since during this period, the DG is not yet re-dispatched, its power remains fixed, with small variations due to its governor actions. This demonstrates the effectiveness of the proposed DHN controls for maintaining frequency stability in the EPN.

4. Conclusions

Detailed dynamic modeling and control of IEHSs in isolated microgrids were developed and validated, with a focus on remote communities. The design and modeling of a DHN to provide space heating in these communities was discussed in detail, based on the utilization of waste heat energy from DG exhaust systems. In this context, the developed dynamic model allowed to analyze the specific insulation needs of the piping for a DHN distribution network in remote areas due to their low linear heat density, which would not be possible using existing static models.

The dynamic IEHS model of the DHN and EPN including HPs was also presented, including a proposed primary and secondary frequency control, offering power reserves for frequency regulation in isolated microgrids for the proper integration of variable RES, taking advantage of the significant thermal energy storage of DHNs. Finally, the feasibility and advantages of using an DHN+EPN IEHS to supply both thermal and electric demand for remote communities was demonstrated through dynamic studies, and by comparing the integrated system with an ETS-based approach. The results show the successful utilization of DHN for meeting thermal requirements and regulating EPN frequency in isolated microgrids with significant penetration of RES. The presented study could be expanded to explore the feasibility of supplying domestic hot water to consumers in remote communities through the DHN.

Funding

This work has been supported by an Egyptian Government Scholarship and NSERC CREATE HyTEM funds.

CRediT authorship contribution statement

Muhammad Abuelhamd: Writing – original draft, Visualization, Validation, Software, Methodology, Investigation, Formal analysis, Data curation. **Claudio A. Cañizares:** Writing – review & editing, Supervision, Resources, Project administration, Methodology, Funding acquisition, Conceptualization.

Declaration of competing interest

The authors declare the following financial interests/personal relationships which may be considered as potential competing interests: Claudio Canizares reports financial support was provided by NSERC Canada. If there are other authors, they declare that they have no known competing financial interests or personal relationships that could have appeared to influence the work reported in this paper.

Data availability

Data will be made available on request.

References

[1] Javanmard ME, Tang Y, Wang Z, Tontiwachwuthikul P. Forecast energy demand, CO2 emissions and energy resource impacts for the transportation sector. Appl Energy 2023;338:120830.

[2] Frison L, Kollmar M, Oliva A, Bürger A, Diehl M. Model predictive control of bidirectional heat transfer in prosumer-based solar district heating networks. Appl Energy 2024;358:122617.

[3] Arriaga M, Cañizares CA, Kazerani M. Northern lights: Access to electricity in Canada's northern and remote communities. IEEE Power Energy Mag 2014;12(4):50–9.

[4] Coady J, Duquette J. Quantifying the impacts of biomass driven combined heat and power grids in northern rural and remote communities. Renew Sustain Energy Rev 2021;148:111296.

[5] Hendricks AM, Wagner JE, Volk TA, Newman DH, Brown TR. A cost-effective evaluation of biomass district heating in rural communities. Appl Energy 2016;162:561–9.

[6] Elsaraf H, Jamil M, Pandey B. Techno-economic design of a combined heat and power microgrid for a remote community in newfoundland Canada. IEEE Access 2021;9:91548–63.

[7] Craig JW, Miller EL, Benowitz J, Manson M, Dumitru T, Hoiland CW. Application of low temperature thermochronology for exploration of blind geothermal systems: A case study from the Kigluaik fault system and pilgrim hot springs, northwestern Alaska. In: PROCEEDINGS, 49th workshop on geothermal reservoir engineering Stanford University, Stanford, California, 2024. 2024.

[8] Yang C, Li Z. Distributed conditional-distributionally robust coordination for an electrical power and flexibility-enhanced district heating system. Appl Energy 2023;347:121491.

[9] Olivares DE, Mehrizi-Sani A, Etemadi AH, Cañizares CA, Iravani R, Kazerani M, Hajimiragha AH, Gomis-Bellmunt O, Saeedifard M, Palma-Behnke R, et al. Trends in microgrid control. IEEE Trans Smart Grid 2014;5(4):1905–19.

[10] Saloux E, Candanedo JA. Model-based predictive control to minimize primary energy use in a solar district heating system with seasonal thermal energy storage. Appl Energy 2021;291:116840.

[11] Poudel B, Gokaraju R. Small modular reactor (SMR) based hybrid energy system for electricity and district heating. IEEE Trans Energy Convers 2021;36(4):2794–802.

[12] Boldrini A, Navarro JJ, Crijns-Graus W, van den Broek M. The role of district heating systems to provide balancing services in the European union. Renew Sustain Energy Rev 2022;154:111853.

[13] Sheng X, Duanmu L. Electricity consumption and economic analyses of district heating system with distributed variable speed pumps. Energy Build 2016;118:291–300.

[14] Yang J, Zhang N, Botterud A, Kang C. On an equivalent representation of the dynamics in district heating networks for combined electricity-heat operation. IEEE Trans Power Syst 2019;35(1):560–70.

[15] Zheng J, Zhou Z, Zhao J, Wang J. Integrated heat and power dispatch truly utilizing thermal inertia of district heating network for wind power integration. Appl Energy 2018;211:865–74.

[16] Zheng W, Hou Y, Li Z. A dynamic equivalent model for district heating networks: Formulation, existence and application in distributed electricity-heat operation. IEEE Trans Smart Grid 2021;12(3):2685–95.

[17] Zhang S, Gu W, Lu S, Yao S, Zhou S, Chen X. Dynamic security control in heat and electricity integrated energy system with an equivalent heating network model. IEEE Trans Smart Grid 2021;12(6):4788–98.

[18] Poudel B, Gokaraju R. Optimal operation of SMR-RES hybrid energy system for electricity and district heating. IEEE Trans Energy Convers 2021;36(4):3146–55.

[19] Korpela T, Kaivosoja J, Majanne Y, Laakkonen L, Nurmoranta M, Vilkko M. Utilization of district heating networks to provide flexibility in CHP production. Energy Procedia 2017;116:310–9.

[20] Iov F, Khatibi M, Bendtsen JD. On the participation of power-to-heat assets in frequency regulation markets—A Danish case study. Energies 2020;13(18):4608.

[21] Harild Rasmussen TB, Wu Q, Zhang M. Primary frequency support from local control of large-scale heat pumps. Int J Electr Power Energy Syst 2021;133:107270.

[22] Calero I, Cañizares CA, Bhattacharya K, Baldick R. Duck-curve mitigation in power grids with high penetration of PV generation. IEEE Trans Smart Grid 2022;13(1):314–29.

[23] Thilker CA, Bacher P, Bergsteinsson HG, Junker RG, Cali D, Madsen H. Non-linear grey-box modelling for heat dynamics of buildings. Energy Build 2021;252:111457.

[24] Larsen HV, Pálsson H, Bøhm B, Ravn HF. Aggregated dynamic simulation model of district heating networks. Energy Convers Manage 2002;43(8):995–1019.

[25] Lopez JMG, Pouresmaeil E, Canizares CA, Bhattacharya K, Mosaddegh A, Solanki BV. Smart residential load simulator for energy management in smart grids. IEEE Trans Ind Electron 2018;66(2):1443–52.

[26] Lim S, Park S, Chung H, Kim M, Baik Y-J, Shin S. Dynamic modeling of building heat network system using simulink. Appl Therm Eng 2015;84:375–89.

[27] Brown CS, Cassidy NJ, Egan SS, Griffiths D. Thermal and economic analysis of heat exchangers as part of a geothermal district heating scheme in the Cheshire Basin, UK. Energies 2022;15(6):1983.

[28] Bergman TL, Bergman TL, Incropera FP, Dewitt DP, Lavine AS. Fundamentals of heat and mass transfer. John Wiley & Sons; 2011.

[29] Maiboom A, Tauzia X, Hétet J-F. Experimental study of various effects of exhaust gas recirculation (EGR) on combustion and emissions of an automotive direct injection diesel engine. Energy 2008;33(1):22–34.

[30] Aghbashlo M, Tabatabaei M, Khalife E, Najafi B, Mirsalim SM, Gharehghani A, Mohammadi P, Dadak A, Shojaei TR, Khounani Z. A novel emulsion fuel containing aqueous nano cerium oxide additive in diesel–biodiesel blends to improve diesel engines performance and reduce exhaust emissions: Part II–exergetic analysis. Fuel 2017;205:262–71.

[31] Borgnakke C, Sonntag RE. Fundamentals of thermodynamics. John Wiley & Sons; 2020.

[32] Capone M, Guelpa E, Verda V. Optimal installation of heat pumps in large district heating networks. Energies 2023;16(3):1448.

[33] van Schijndel AWM. Integrated heat air and moisture modeling and simulation (Ph.D. thesis), Technische Universiteit Eindhoven Eindhoven; 2007.

[34] Törnros T, Resch B, Rupp M, Gündra H. Geospatial analysis of the building heat demand and distribution losses in a district heating network. ISPRS Int J Geo-Inf 2016;5(12):219.

[35] PVWatts Calculator, https://pvwatts.nrel.gov/pvwatts.php.

[36] Census of Population, https://www12.statcan.gc.ca.

[37] What is THERMOS?, https://www.thermos-project.eu/thermos-tool/what-is-thermos/.

[38] Geology Soil Geochem Surv Rpt., https://www.geologyontario.mines.gov.on.ca/.

[39] Zhang L, Wang Z, Yang X, Jin L, Zhang Q, Hu W. Thermo-economic analysis for directly-buried pipes insulation of district heating piping systems. Energy Procedia 2017;105:3369–76.

[40] Abu-Hamdeh NH, Khdair AI, Reeder RC. A comparison of two methods used to evaluate thermal conductivity for some soils. Int J Heat Mass Transfer 2001;44(5):1073–8.

[41] 3512 diesel generator sets electric power. Caterpillar Inc., https://www.wpowerproducts.com/wp-content/uploads/2020/08/CM20181219-11054-44856.pdf.

[42] Jakubek D, Ocłoń P, Nowak-Ocłoń M, Sułowicz M, Varbanov PS, Klemeš JJ. Mathematical modelling and model validation of the heat losses in district heating networks. Energy 2023;267:126460.

[43] Simscape Electrical, https://www.mathworks.com/help/sps/.

[44] Farrokhabadi M, Cañizares CA, Bhattacharya K. Frequency control in isolated/islanded microgrids through voltage regulation. IEEE Trans Smart Grid 2015;8(3):1185–94.

[45] De Brito MA, Sampaio LP, Luigi G, e Melo GA, Canesin CA. Comparative analysis of MPPT techniques for PV applications. In: IEEE international conference on clean electrical power. ICCEP, 2011, p. 99–104.

[46] Arriaga M, Cañizares C. Overview and analysis of data for microgrid at Kasabonika lake first nation. hatch project confidential report, University of Waterloo, tech. rep, KLFN, 2015.

[47] Solanki BV, Cañizares CA, Bhattacharya K. Practical energy management systems for isolated microgrids. IEEE Trans Smart Grid 2018;10(5):4762–75.

[48] Sauter PS, Solanki BV, Canizares CA, Bhattacharya K, Hohmann S. Electric thermal storage system impact on northern communities' microgrids. IEEE Trans Smart Grid 2017;10(1):852–63.

[49] Devia W, Agbossou K, Cardenas A. An evolutionary approach to modeling and control of space heating and thermal storage systems. Energy Build 2021;234:110674.

[50] Bedouani BY, Moreau A, Parent M, Labrecque B. Central electric thermal storage (ETS) feasibility for residential applications: Part 1. Numerical and experimental study. Int J Energy Res 2001;25(1):53–72.

[51] Mendieta W, Cañizares CA. Primary frequency control in isolated microgrids using thermostatically controllable loads. IEEE Trans Smart Grid 2020;12(1):93–105.

[52] Curtis D, Singh B. Northern microgrid project–a concept. In: World Energy Congress. Montreal, Canada; 2010.